Article

Sliding Mode Speed Control in Synchronous Motors for Agriculture Machinery: A Chattering Suppression Approach

David Marcos-Andrade [1], Francisco Beltran-Carbajal [2,*], Ivan Rivas-Cambero [1], Hugo Yañez-Badillo [3], Antonio Favela-Contreras [4] and Julio C. Rosas-Caro [5]

[1] Departamento de Posgrado, Universidad Politécnica de Tulancingo, Tulancingo 43629, Mexico; david.marcos2315006@upt.edu.mx (D.M.-A.); ivan.rivas@upt.edu.mx (I.R.-C.)

[2] Departamento de Energía, Unidad Azcapotzalco, Universidad Autónoma Metropolitana, Azcapotzalco, Mexico City 02200, Mexico

[3] Departamento de Investigación, TecNM: Tecnologico de Estudios Superiores de Tianguistenco, Tianguistenco 52650, Mexico; hugo_mecatronica@test.edu.mx

[4] Tecnologico de Monterrey, School of Engineering and Sciences, Monterrey 64849, Mexico; antonio.favela@tec.mx

[5] Facultad de Ingeniería, Universidad Panamericana, Álvaro del Portillo 49, Zapopan 45010, Mexico; crosas@up.edu.mx

* Correspondence: fbeltran@azc.uam.mx

Abstract: Synchronous motors have extended their presence in different applications, specifically in high-demand environments such as agronomy. These uses need advanced and better control strategies to improve energy efficiency. Within this context, sliding mode control has demonstrated effectiveness in electric machine control due to its advantages in robustness and quick adaptation to uncertain dynamic system disturbances. Nevertheless, this control technique presents the undesirable chattering phenomenon due to the discontinuous control action. This paper introduces a novel speed integral control scheme based on sliding modes for synchronous motors. This approach is designed to track smooth speed profiles and is evaluated through several numeric simulations to verify its robustness against variable torque loads. This approach addresses using electric motors for different applications such as irrigation systems, greenhouses, pumps, and others. Moreover, to address the chattering problem, different sign function approximations are evaluated in the control scheme. Then, the most effective functions for suppressing the chattering phenomenon through extensive comparative analysis are identified. Integral compensation in this technique demonstrates improvement in motor performance, while sign function approximations show a chattering reduction. Different study cases prove the robustness of this control scheme for large-scale synchronous motors. The simulation results validate the proposed control scheme based on sliding modes with integral compensation, by achieving chattering reduction and obtaining an efficient control scheme against uncertain disturbances in synchronous motors for agronomy applications.

Keywords: automation; agricultural machinery; synchronous motor control; sliding mode control; chattering suppression; sign function

1. Introduction

Permanent Magnet Synchronous Motors (PMSMs) can be found in many automated systems because they provide high-efficiency technology, mainly power and energy reliability. In this sense, this electrical machine is an excellent option to power agronomy systems. Control schemes must be robust, achieving better responses against uncertain dynamical disturbances. In [1], a speed controller based on sliding modes with an improved exponential reaching law and proportional resonance strategy is proposed for a PMSM system within the electric vehicle context. This approach is used to address the chattering problem and improve system response. The different control schemes in PMSM

will present different behaviors depending on switching techniques on control drivers. The field-oriented control and different strategies such as look-up tables mixed with traditional Proportional–Integral (PI) controllers to improve technique implementation focused on using it in electric vehicles, as shown in [2]. In this context, electrical motors are subjected to uncertain dynamic disturbances where the control schemes should respond quickly to compensate for these issues. Schemes such as the adaptive super-twisting nonlinear Fractional-Order Proportional–Integral–Derivative and sliding mode control for speed regulation are used to weaken the chattering phenomenon by implementing an adaptive super-twisting reaching law approach, as proposed in [3]. Also, a backstepping control based on sliding modes can be applied to asynchronous machines for similar purposes, as shown in [4]. These control schemes can board non-linearities present in electric machines.

Sliding mode control (SMC) is known to exhibit an issue termed chattering. Various strategies have been proposed to mitigate this problem. In this context, the phenomenon is mathematically defined in [5], utilizing a range of signals and offering a comprehensive explanation of sliding surfaces. Additionally, in [6], the presence of singularities and chattering in sliding mode control is addressed by introducing an approach that centers on eliminating derivative terms within the control law and devising a continuous control strategy. In this context, electric machine control is commonly implemented in speed control devices such as inverters or Variable Frequency Drivers (VFDs); SMC can be used in different rotational machine drivers, as is demonstrated in [7]. This study focuses on designing a torque ripple control based on sliding modes for a switched reluctance motor. Moreover, different strategies can be employed to increase sliding mode control robustness for multiple applications. Generalized PI control mixed with this technique can demonstrate optimal behavior, specifically in vibration attenuation problems in automotive suspension systems [8]. In this way, improving system response performance by strategies such as fast non-singular terminal sliding mode and adding state observers allow for faster system response [9]. In addition to this proposal, Super-Twisting Sliding Mode Control, such as that proposed in [10], is a good choice for developing speed control strategies in electrical machines. However, this control must still solve the chattering problem. For this purpose, different studies have developed different versions of the sign function as an alternative solution to this problem [11–14], and they are utilized in this manuscript. Control systems can be located in a wide range of applications in different environments. The increase in automation in recent decades entails a precise knowledge of control strategies for systems such as rotational machinery, robotics arms, irrigation, industrial processes, agronomy, and others. Different control design procedures can be used for linear and nonlinear systems for these purposes. PI and PID control are the most common strategies to manipulate a desired system output [15]. However, sliding mode control is increasing its presence in this class of systems due to robustness against uncertainties. Different design strategies involving stability analysis and sliding surfaces can be selected for different performance requirements, as is demonstrated in books [16,17]. This control technique is easy to implement and can deal with uncertainty for precision irrigation applications. To reduce the chattering phenomenon, sign function approximation demonstrates simplicity and good performance [18].

Often, control schemes are designed under assumptions of different unknown uncertain disturbances in synchronous motors. These issues have been addressed by online estimation techniques to improve control behavior, and these approaches allow the identification of different load torque parameters under various conditions [19,20]. Additionally, artificial intelligence integration in sliding mode control schemes increases efficiency and robustness; ref. [21] proposes a new adaptive-like neural control strategy for electromagnetic suspension systems where the algorithm approximates discontinuous control action. Furthermore, techniques such as adaptive fuzzy control also demonstrate practical implementation and effectiveness for synchronous motors; adaptability allows non-linearity approximation, improving control scheme [22]. Electric tractors with new steering structures can improve operation efficiency in the context of machinery for agriculture applications.

These autonomous vehicles operate under hard conditions where parameter changes and disturbances are present. To solve these issues, sliding mode control demonstrates better behavior in comparison with the PID technique under common conditions such as serpentine, double line shift, and step [23,24]. In the same way, electric motors power these autonomous vehicles. Slip problems in agricultural vehicles are present due to environmental conditions; consequently, torque control is needed for each wheel. Integrating PI and sliding mode technique control with pertinent parameter acquisition allows the correct torque to be delivered to the wheels for tracking tasks [25]. Some fertigation machines are powered by asynchronous motors. For this application, load disturbances are present in the system, where a load torque observer for adjusting sliding mode control parameters demonstrates fluctuation reduction and robustness against disturbances [26]. Analysis through simulations can provide a general perspective of real systems. However, experimental implementations present issues due to the nature of real systems; synchronous motors are present in electric vehicles where experimental analysis provides proportionate parameters to compare and validate different control strategies [27,28]. In this sense, a rigorous review of different speed control techniques for PMSM is conducted in [29], emphasizing methods to obtain robustness, giving mathematical tools to facilitate the design, and comparing each review technique's advantages. Also, ref. [30] proposes a solution to obtain high-precision control for low speeds in PMSM based on a novel iterative learning controller used to reject disturbances.

To implement control schemes in synchronous motors, initial position methods have been proposed to start the motor; in [31], a method to calculate the initial position is proposed using frequency signals and a simple linear formula. Moreover, The efficient and robust tracking of planned references within a PID control scheme is addressed in [32] for synchronous generators. Also, the synchronous motor mathematical model is commonly transformed under the $dq0$ reference frame. However, most physical algorithms require employing this transform to implement control schemes. In this context, ref. [33] conducts experimental tests to evaluate the dq-axis time reaction in different platforms. These data could be considered in control schemes since simulation evaluations do not consider computational costs in real implementations. In addition, using sign function approximations have improved Sliding Mode Observers [34–36], and sensorless control strategies for PMSM used in electric vehicles [37]. Finally, in ref. [38], a control method for low-speed high-torque PMSM is proposed, combining nonlinear feedback, integral sliding mode, and a sliding mode observer to reduce chattering.

Electrical motors are increasing their presence in agricultural machinery like tractors, irrigation, and fertigation systems. The improvement in control strategies entails better resource utilization. Thus, achievements such as water conservation, correct fertilizer distribution, improvement in electric agriculture vehicles, and others are made. In this research paper, a novel control scheme based on sliding mode control with integral compensation for tracking smooth speed profiles in synchronous motors for agriculture applications is proposed. To address uncertain dynamical disturbances, different variable torque loads are evaluated to validate the control robustness. This approach can address the dynamic uncertainties present in agricultural environments. In contrast with different important techniques for suppressing the chattering phenomenon, using sign function approximations keeps this control technique easy to implement. Moreover, using abrupt references such as steps could present issues, as physical systems cannot quickly change from one state to another. To avoid these problems, smooth speed profiles are proposed using Bezier curves to obtain a softer response and optimal system behavior. Furthermore, changes in speed trajectories are involved to verify the control scheme reaction to different conditions. Various study cases are evaluated through numeric simulations using different continuous sign function versions in a Matlab environment. The simulation results demonstrate the robustness against uncertain dynamical disturbances and chattering reduction in the proposed control scheme.

The manuscript is organized as follows. In Section 2, continuous sing function versions are presented in an illustrative sliding mode control scheme for an irrigation system to demonstrate how these approximations can suppress chattering while the slope is manipulated. Section 3 is focused on describing the speed control design for the PMSM. In Section 4, simulation results and discussion are conducted, different study cases with different speed trajectories are proposed, and control scheme robustness is validated through optimal response against different variable torques. Lastly, in Section 5, conclusions are described.

2. Sign Function Approximations as a Solution to Mitigate Chattering Phenomenon

The chattering phenomenon is described as finite-frequency, finite-amplitude oscillations appearing in many sliding mode implementations. These oscillations are caused by the high-frequency switching of the sliding mode controller [16]. For this paper, the standard sign function is denoted as follows:

$$sign_1(\sigma) = \begin{cases} -1 & \text{if } \sigma < 0 \\ 0 & \text{if } \sigma = 0 \\ 1 & \text{if } \sigma > 0 \end{cases} \tag{1}$$

where σ is the sliding surface within the SMC context. This function is handy in various mathematical and computational applications. The sign function helps design control laws that exhibit robustness and stability against uncertainties and disturbances in systems characterized by discontinuities. At this point, the chattering phenomenon appears, leading to challenges in control implementation. Using the sign function in sliding mode control schemes causes abrupt controller switching, resulting in rapid changes in the control output. In certain cases, if the physical limitations of the system are not considered or the controller operates near the system's limits, the presence of chattering can become more pronounced [11,14].

An illustrative example demonstrates how to mitigate the chattering problem inherent in this control technique by using sign function approximations. Consider the irrigation system depicted in Figure 1. The water tank is fed from a nearby water source; according to [18], the pressure uncertainties occur due to the tank water level. The valve is controlled by a DC motor that controls the open position for irrigation needs.
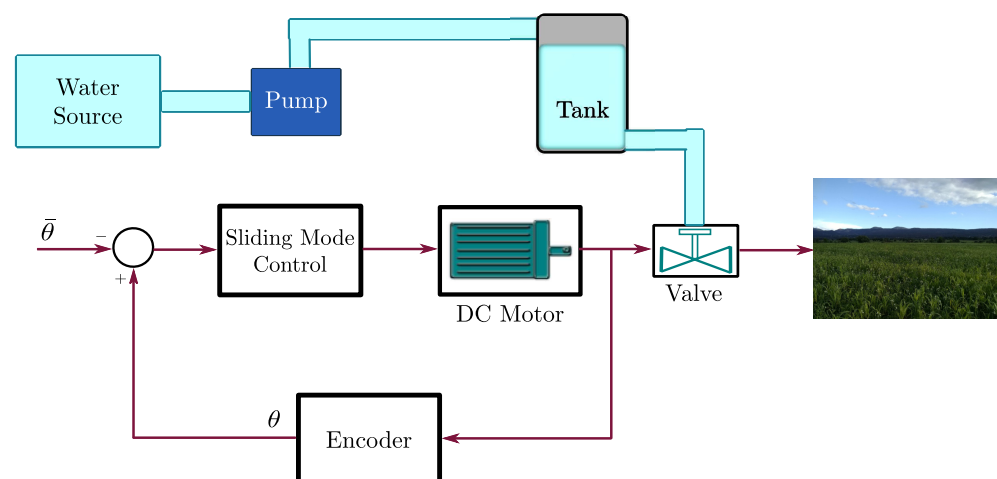

Figure 1. Control scheme for an irrigation system for a valve controlled by DC motor.

Sliding mode control is introduced to deal with the load on the control valve due to hydrostatic pressure, water level in the tank, and temperature variations producing

uncertainties. A DC motor controls the valve, and the mathematical model for the plant is given by

$$\ddot{\theta} + 43.06\dot{\theta} + 7.128\theta = 326.2u \tag{2}$$

where θ represents the DC motor's position to control the valve, and u is the control input [18]. Now, for simulation purposes, the sliding surface selected for the system is

$$\sigma = ce + \dot{e} \tag{3}$$

with $c > 0$. For regulation tasks, the error is defined as

$$e = \theta - \bar{\theta} \tag{4}$$
$$\dot{e} = \dot{\theta} \tag{5}$$

with $\bar{\theta}$ as the desired constant position. The control law is described as follows:

$$u = u_0 sign_1(\sigma) \tag{6}$$

where $u_0 > 0$. The discontinuous action in the control implies generating the chattering phenomenon. This effect becomes evident when utilizing specific system parameters, such as $\bar{\theta} = 5$ for the DC motor position depicted in Figure 2, where the manifestation of chattering is noticeable.
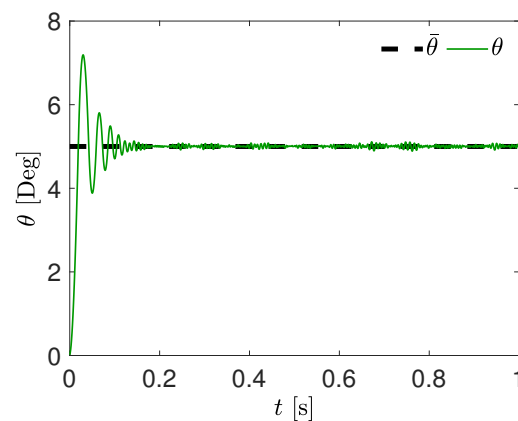

Figure 2. Valve DC motor position response with chattering phenomenon for the irrigation system. $\bar{\theta}$ for the desired constant position and, θ as the read position.

Different sign function approximations are designed to reduce the impact of abrupt changes in the control action; see Equations (7)–(13). The parameter ϵ can be adjusted to manipulate the function slope. When this value tends to zero, the approximation is more similar to the sign function; see Figure 3a. When this parameter is increased, the slope of the function becomes steeper; see Figure 3b. This effect helps to reduce the chattering phenomenon [11–14]. However, the sign function in sliding mode control is used to address non-linearities and uncertainties. So if ϵ is a big value, the slope of the function is steeper. Therefore, the approximation moves away from the sign function. This could affect addressing non-linearities. After the control design, approximations consist of only substituting the sign function by any approximation. Then, the selection of the ϵ value can be performed empirically. However, in some cases, this can be addressed as an optimization problem where the objective is to minimize the error by reducing the non-desired oscillations.

$$\text{sign}_2(\sigma) = \frac{\sigma}{|\sigma| + \epsilon} \tag{7}$$

$$\text{sign}_3(\sigma) = \frac{2}{1 + e^{-\frac{\sigma}{\epsilon}}} - 1 \tag{8}$$

$$\text{sign}_4(\sigma) = \tanh\frac{\sigma}{\epsilon} \tag{9}$$

$$\text{sign}_5(\sigma) = \frac{2}{\pi}\arctan\frac{\sigma}{\epsilon} \tag{10}$$

$$\text{sign}_6(\sigma) = \frac{\frac{\sigma}{\epsilon}}{\sqrt{1 + \left(\frac{\sigma}{\epsilon}\right)^2}} \tag{11}$$

$$\text{sign}_7(\sigma) = \frac{\sigma}{\sqrt{\sigma^2 + \epsilon}} \tag{12}$$

$$\text{sign}_8(\sigma) = \begin{cases} \dfrac{\sigma}{\epsilon} & \text{if } |\sigma| \le \epsilon \\ \text{sign}_1(\sigma) & \text{if } |\sigma| > \epsilon \end{cases} \tag{13}$$
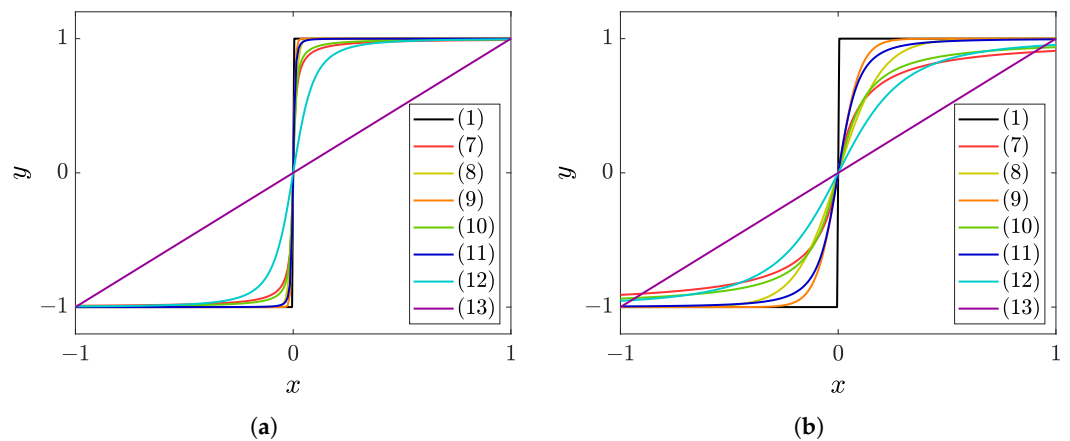

Figure 3. Different normalized approximations in $[-1, 1]$ compared to the standard sign function. (**a**) Approximations from (7)–(13) with $\epsilon = 0.01$. (**b**) Approximations from (7)–(13) with $\epsilon = 0.1$.

Now consider the system response displayed in Figure 2. Adopting any sign function approximation, for example, Equation (8) with an $\epsilon = 0.5$, the chattering phenomenon can be effectively reduced, as demonstrated in Figure 4. Notice that although this system presents uncertainties, external disturbances are not considered in the model.

Integrating continuous sign function approximations into a sliding mode control design offers an efficient implementation by replacing the standard sign function. This adaptation brings significant advantages, particularly in systems with electric machines, where control schemes are commonly deployed in power devices such as VFDs and inverters. These systems often experience oscillatory components in their generated signals due to the action of switching devices. The reduction in or elimination of the chattering phenomenon, achieved through this approach, results in a better response, as demonstrated in this study.
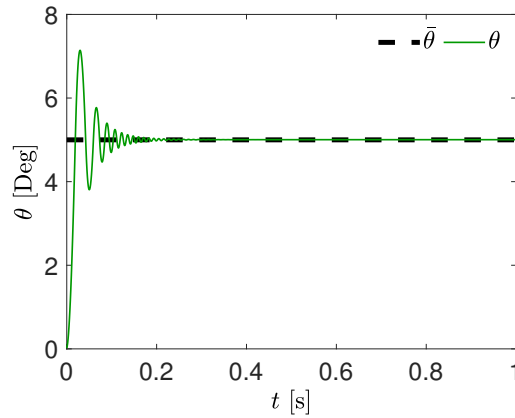
Figure 4. Valve DC motor position response employing sign function approximation (8) to mitigate chattering. $\bar{\theta}$ for the desired constant position and, θ as the read position.

3. Integral Sliding Mode Control Design for Permanent Magnet Synchronous Motor Speed Control

This section describes the control scheme designed for tracking speed profiles for PMSM from the dynamical model transformed under $dq0$ reference frame to obtain the control voltages. The design of the controller is carried out as follows: the controller development for the direct axis (referred to as the 'd' axis) and, subsequently, the quadrature axis controller (denoted as the 'q' axis). The control scheme design involves tracking smooth reference speed profiles, such that applications of these motors in fertigation systems, pumps, irrigation, electric agriculture vehicles, and others entail precision and adequate response under uncertainties. Furthermore, the system's response to external disturbances can be improved by adding integral compensation in sliding surfaces. This control strategy minimizes speed-tracking errors, and contributes to the system's robustness, enabling the controller to maintain stable performance despite uncertain disturbances.

3.1. Dynamical Model of Permanent Magnet Synchronous Motor

For this study, synchronous motor nonlinear dynamics is transformed using the reference frame $dq0$, according to Clarke and Park matrices of Equation (14). By converting the nonlinear motor dynamics (*abc*) into a specific reference frame, often the stationary $dq0$ reference frame, the variables and equations align with the physical orientation of the motor. This transformation can be visualized in Figure 5.

$$T_{\text{Clarke}} = \begin{bmatrix} \frac{2}{3} & -\frac{1}{\sqrt{3}} & \frac{1}{\sqrt{3}} \\ 0 & \frac{2}{\sqrt{3}} & \frac{1}{\sqrt{3}} \\ \frac{1}{\sqrt{2}} & \frac{1}{\sqrt{2}} & \frac{1}{\sqrt{2}} \end{bmatrix} \qquad T_{\text{Park}}(\theta) = \begin{bmatrix} \cos(\theta) & \sin(\theta) & 0 \\ -\sin(\theta) & \cos(\theta) & 0 \\ 0 & 0 & 1 \end{bmatrix} \qquad (14)$$

This approach simplifies the analysis and control design process [20]. Control laws designed in a properly chosen reference frame often become simpler. This simplification can lead to more efficient control algorithms, making them easier to implement and tune.

The mathematical model for developing the control scheme is

$$\frac{d}{dt}i_d = -\frac{R_s}{L_d}i_d + \frac{PL_q}{L_d}i_q\omega + \frac{1}{L_d}u_d \qquad (15)$$

$$\frac{d}{dt}i_q = -\frac{R_s}{L_q}i_q - \frac{PL_d}{L_q}i_d\omega - \frac{P\lambda_m}{L_q}\omega + \frac{1}{L_q}u_q \qquad (16)$$

$$J\frac{d}{dt}\omega = \frac{3}{2}P\lambda_m i_q - b\omega - \tau_L \qquad (17)$$

i_d and i_q represent the electric current signals in the direct and quadrature axes, respectively, and the motor shaft angular velocity is denoted by ω. L_d is the direct axis inductance, L_q is

the quadrature axis inductance, R_s is the armature resistance, J is the moment of inertia, and b is the viscous damping coefficient. The number of pole pairs is indicated as P, and the magnetic flux of the permanent magnet is denoted by λ_m. τ_L describes the variable load torque affecting the motor rotor dynamics. For this study, it is assumed that $L_d = L_q$.
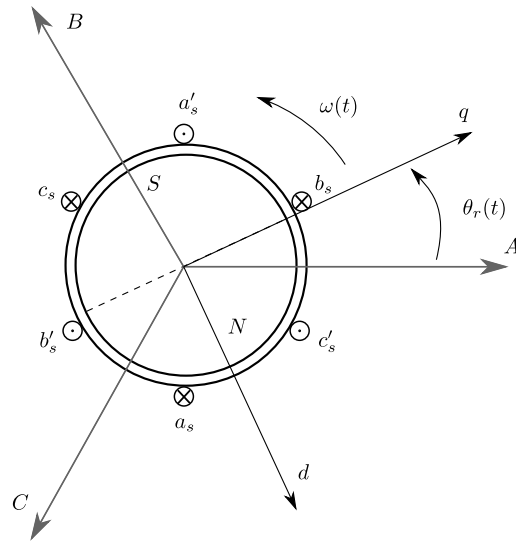

Figure 5. Illustrative example of $dq0$ reference frame for a Permanent Magnet Synchronous Motor.

3.2. Motor Control Design for Direct Current Axis

The control design for the synchronous motor aims to ensure the motor operates with optimal performance by providing appropriate voltages. Initially, the focus is on a controller dedicated to the direct axis current. The controller's primary objective is to maintain a reference trajectory, where a predefined $i_d^\star = 0$ is set, strategically aimed at simplifying the angular speed controller's operation and enhancing efficiency. The direct axis current tracking error is the difference between the reference and actual value $e_d = i_d - i_d^\star$.

The selected sliding surface is given as

$$
\begin{aligned}
\sigma_d = e_d &+ \alpha_{(r,d)} \int_{t_0} e_d + \alpha_{(r-1,d)} \int_{t_0}^{(2)} e_d + \alpha_{(r-2,d)} \int_{t_0}^{(3)} e_d \\
&+ \cdots + \alpha_{(1,d)} \int_{t_0}^{(r-1)} e_d + \alpha_{(0,d)} \int_{t_0}^{(r)} e_d
\end{aligned}
\tag{18}
$$

where the notation $\int_{t_0}^{(r)} e$ denotes the r-th iterated integral of the form $\int_{t_0}^{t} \int_{t_0}^{\tau_1} \cdots \int_{t_0}^{\tau_{r-1}} e(\tau_r) \, d\tau_r \cdots d\tau_1$, as is shown in [32]. The sliding surface described by σ_d establishes the system and takes direct axis current to reference tracking $i_d^\star$ to obtain a better behavior against uncertainties. Integral compensation can be added to obtain the system's response to cero. Now, the dynamics for the sliding surface are given by

$$
\begin{aligned}
\frac{d}{dt} \sigma_d = \frac{d}{dt} e_d &+ \alpha_{(r,d)} e_d + \alpha_{(r-1,d)} \int_{t_0} e_d + \alpha_{(r-2,d)} \int_{t_0}^{(2)} e_d \\
&+ \cdots + \alpha_{(1,d)} \int_{t_0}^{(r-2)} e_d + \alpha_{(0,d)} \int_{t_0}^{(r-1)} e_d
\end{aligned}
\tag{19}
$$

Substituting Equation (15) in Equation (19), we obtain

$$
\begin{aligned}
\frac{d}{dt} \sigma_d = &-\frac{R_s}{L_d} i_d + \frac{P L_q}{L_d} i_q \omega + \frac{1}{L_d} u_d - \frac{d}{dt} i_d^\star + \alpha_{(r,d)} e_d + \alpha_{(r-1,d)} \int_{t_0} e_d \\
&+ \alpha_{(r-2,d)} \int_{t_0}^{(2)} e_d + \cdots + \alpha_{(1,d)} \int_{t_0}^{(r-2)} e_d + \alpha_{(t_0,d)} \int_{t_0}^{(r-1)} e_d
\end{aligned}
\tag{20}
$$

In order to tune the parameters α, the next stable r-th order polynomial is proposed:

$$P_d(s) = (s + \alpha_d)^r \tag{21}$$

Finally, the direct-axis controller denoted as u_d is obtained as follows:

$$
\begin{aligned}
L_d u_d = {} & \frac{d}{dt}i_d^\star + \frac{R_s}{L_d}i_d - \frac{PL_q}{L_d}i_q\omega - \alpha_{(r,d)}e_d - \alpha_{(r-1,d)}\int_{t_0} e_d - \alpha_{(r-2,d)}\int_{t_0}^{(2)} e_d \\
& - \cdots - \alpha_{(1,d)}\int_{t_0}^{(r-2)} e_d - \alpha_{(0,d)}\int_{t_0}^{(r-1)} e_d - W_d sign_1(\sigma_d)
\end{aligned}
\tag{22}
$$

3.3. Speed Motor Control Design for Quadrature Current Axis

Next, Equation (17) is taken and is derived with respect to time, obtaining

$$\frac{d^2}{dt^2}\omega = \frac{3}{2}\frac{P\lambda_m}{J}\frac{d}{dt}i_q - \frac{b}{J}\frac{d}{dt}\omega - \frac{1}{J}\frac{d}{dt}\tau_L \tag{23}$$

Subsequently, Equation (16) is introduced into the derivative value, obtaining

$$\frac{d^2}{dt^2}\omega = -\frac{3}{2}\frac{P\lambda_m R_s}{JL_q}i_q - \frac{3}{2}\frac{P^2\lambda_m L_d}{JL_q}i_d\omega - \frac{3}{2}\frac{P^2\lambda_m^2}{JL_q}\omega + \frac{3}{2}\frac{P\lambda_m}{JL_q}u_q - \frac{b}{J}\frac{d}{dt}\omega - \frac{1}{J}\frac{d}{dt}\tau_L \tag{24}$$

Now, the speed error is given by $e = \omega - \omega^\star$, where $\omega^\star$ represents the motor's angular speed reference trajectory. The proposed sliding surface for tracking trajectories is selected as

$$
\begin{aligned}
\sigma_q = {} & \frac{d}{dt}e_\omega + \alpha_{(r,q)}e_\omega + \alpha_{(r-1,q)}\int_{t_0} e_\omega + \alpha_{(r-2,q)}\int_{t_0}^{(2)} e_\omega + \alpha_{(r-3,q)}\int_{t_0}^{(3)} e_\omega \\
& + \cdots + \alpha_{(1,q)}\int_{t_0}^{(r-1)} e_\omega + \alpha_{(0,q)}\int_{t_0}^{(r)} e_\omega
\end{aligned}
\tag{25}
$$

and the surface dynamics is given by

$$
\begin{aligned}
\frac{d}{dt}\sigma_q = {} & \frac{d^2}{dt^2}e_\omega + \alpha_{(r,q)}\frac{d}{dt}e_\omega + \alpha_{(r-1,q)}e_\omega + \alpha_{(r-2,q)}\int_{t_0} e_\omega + \alpha_{(r-3,q)}\int_{t_0}^{(2)} e_\omega \\
& + \cdots + \alpha_{(1,q)}\int_{t_0}^{(r-2)} e_\omega + \alpha_{(0,q)}\int_{t_0}^{(r-1)} e_\omega
\end{aligned}
\tag{26}
$$

A stable polynomial of degree $r + 1$ is selected in order to tune α_q parameters.

$$P_q(s) = (s + \alpha_q)^{r+1} \tag{27}$$

The iterated integrals allow for an increase in the controller robustness. Ultimately, the complete controller for the quadrature axis is derived from Equation (24), obtaining

$$
\begin{aligned}
\rho u_q = {} & \frac{d^2}{dt^2}\omega^\star + \frac{3}{2}\frac{P\lambda_m R_s}{JL_q}i_q + \frac{3}{2}\frac{P^2\lambda_m L_d}{JL_q}i_d\omega + \frac{3}{2}\frac{P^2\lambda_m^2}{JL_q}\omega + \frac{b}{J}\frac{d}{dt}\omega + \frac{1}{J}\frac{d}{dt}\tau_L \\
& - \alpha_{(r,q)}\frac{d}{dt}e_\omega - \alpha_{(r-1,q)}e_\omega - \alpha_{(r-2,q)}\int_{t_0} e_\omega - \alpha_{(r-3,q)}\int_{t_0}^{(2)} e_\omega \\
& - \cdots - \alpha_{(1,q)}\int_{t_0}^{(r-2)} e_\omega - \alpha_{(0,q)}\int_{t_0}^{(r-1)} e_\omega - W_q sign_1(\sigma_q)
\end{aligned}
\tag{28}
$$

with

$$\rho = \frac{2}{3}\frac{JL_q}{P\lambda_m} \tag{29}$$

The proposed control scheme is designed considering oscillatory torque loads to which the motor is commonly subjected. Notice that τ_L is present in Equation (28), so W_q should be selected such that

$$W_q > \left| \frac{1}{J} \frac{d}{dt} \tau_L \right| \tag{30}$$

The diagram in Figure 6 describes the process as follows. The speed and current references $i_d^\star$ and $\omega^\star$ are planned as displayed in the next section by Bézier curves. Currents and velocity are obtained from the electrical machine; the three-phase currents are transformed under matrices of Equation (14). Once ω and i_d are obtained, the tracking errors can be computed and then they are processed on the sliding surfaces σ_d, σ_q. The discontinuous action in the controllers is substituted in the control action, aiming to mitigate the chattering phenomenon. Finally, the control signals u_d, u_q can be used to generate the control signals that the three-phase inverter will deliver to PMSM. However, this study is only focused on analyzing how approximations can reduce the chattering phenomenon.
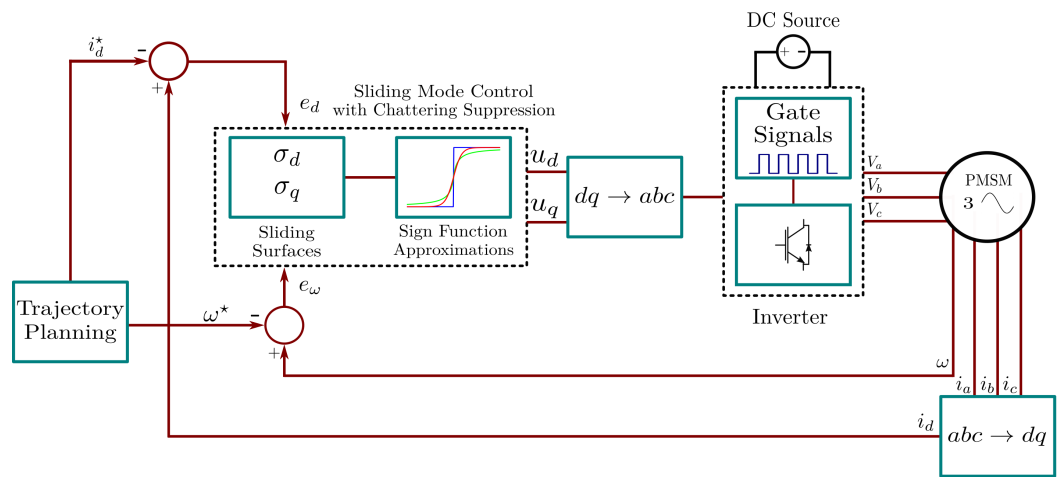
Figure 6. Proposed sliding mode speed control scheme with chattering reduction for PMSM.

4. Simulation Results and Discussion

Several simulations utilizing MATLAB software version 2020a were conducted to validate the analytical results obtained. The numerical method used was Runge–Kutta–Felberg, with a step size of 1 ms; 10-hp synchronous motor parameters were used for this study, as shown in Table 1 [19].

Table 1. 10-hp synchronous motor parameters for study cases.

Parameter	Value
R_s	2.6 Ω
L_d	6.73 H
L_q	L_d
λ_m	0.319 Wb
P	2
b	0.0005 Nm s
J	3.5×10^{-5} Kg m^2

For many applications in the agriculture context, synchronous motors are subjected to hard operation conditions. In this sense, the load torque shown in Figure 7 is proposed and is expressed by Equation (30), and its parameter values are displayed in Table 2. This approach involved subjecting the system to varying load conditions, ensuring that the control design remains effective and stable despite changing external forces.

$$\tau_L = \sum_{i=1}^{4} A_i \sin(\omega_i t) \tag{31}$$

Table 2. Parameter values of load torque proposed as an oscillation addition.

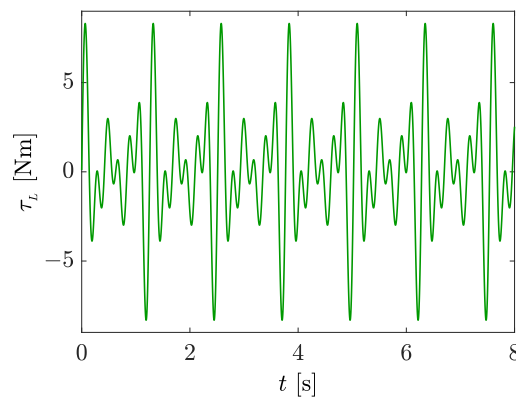| Parameter	Value
Amplitude	(Nm)
A_1	2.5
A_2	2
A_3	2
A_4	2.5
Frequency	(rad/s)
ω_1	15
ω_2	20
ω_3	25
ω_4	30

Figure 7. Load torque proposed for evaluating the control scheme robustness in the first study case.

Moreover, the speed trajectory reference $\omega^\star$ is proposed by Bézier curves within the controller's scheme. These curves offer a method to attain smooth changes in the speed trajectory over a defined time interval $[t_1, t_2]$. By using Bézier curves, the controller achieves gradual and continuous adjustments in the speed reference, useful in many applications. Equation (32) describes the speed trajectory for the first comparisons.

$$\omega^\star = \begin{cases} \overline{\omega}_1 & \text{for } 0 \leq t \leq t_1 \\ \overline{\omega}_1 + (\overline{\omega}_2 - \overline{\omega}_1)\mathfrak{B}_\omega & \text{for } t_1 < t < t_2 \\ \overline{\omega}_2 & \text{for } t_2 \leq t \leq t_3 \\ \overline{\omega}_2 + (\overline{\omega}_3 - \overline{\omega}_2)\mathfrak{B}_\omega & \text{for } t_3 < t < t_4 \\ \overline{\omega}_3 & \text{for } t \geq t_4 \end{cases} \tag{32}$$

where $\overline{\omega}_1 = 0$ rad/s, $\overline{\omega}_2 = 104.719$ rad/s (1000 rpm), $\overline{\omega}_3 = 157.079$ rad/s (1500 rpm), $t_1 = 0$ s, $t_2 = 2$ s, $t_3 = 4$ s, $t_4 = 5$ s, $\mathfrak{B}_\omega$ is the Bézier curve described by

$$\mathfrak{B}_\omega = \sum_{k=1}^{9} r_k \left(\frac{t - t_1}{t_2 - t_1} \right)^{2+k} \tag{33}$$

Figure 8 illustrates the initial speed trajectory for the first study case. Then, each approximation described previously is tested by substituting the standard sign function ($sign_1$), thereby facilitating an evaluation to determine the most suitable one that demonstrates optimal behavior in the system's response.
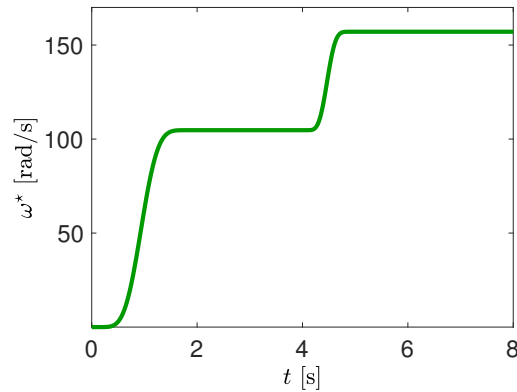
Figure 8. Speed reference trajectory for the first study case.

4.1. Control Scheme Evaluation for the First Speed Trajectory

Figure 9 illustrates that using the standard sign function introduces a noticeable chattering effect in the motor's speed response, as depicted in Figure 9a. Chattering, characterized by rapid fluctuations, affects the system's performance. These variations in the speed response can lead to undesired vibrations and mechanical stress on the motor and its connected systems. In Figure 9b,c, an analysis of the direct axis and quadrature axis voltages reveals the presence of this phenomenon in each respective control signal. However, it is noticeable that the control scheme exhibits adequate behavior against the variable torque.

(**a**)

(**b**)

(**c**)
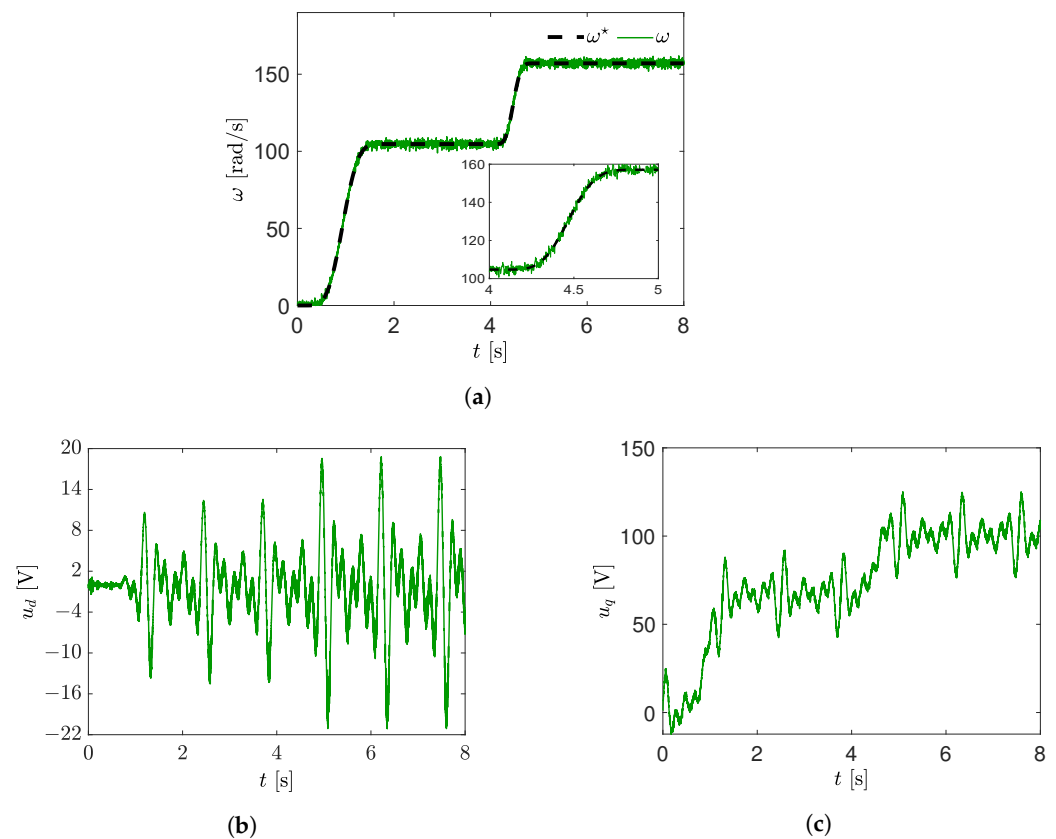
Figure 9. Motor synchronous control parameter output using standard sign function (1). (**a**) Speed response with chattering phenomenon, first trajectory planned, and synchronous motor speed response. (**b**) Voltage generated in direct axis, (**c**) voltage generated in quadrature axis.

4.2. Sign Function Approximation Evaluation with the First Speed Trajectory

Next, the initial continuous approximation (7) is inserted into the control law. The manipulation of the ϵ parameter can reduce considerably the chattering phenomenon, as is demonstrated in Figure 10. Adjusting the ϵ parameter results in a softer slope, achieving a smoother transition around the zero value and reducing the chattering effect. It is essential to strike a balance in selecting the appropriate ϵ value. A very high value of ϵ might lead to a function that deviates significantly from the actual sign function, thus affecting the system's intended performance. Conversely, a smaller ϵ value may result in similarly abrupt changes, failing to reduce the chattering effect sufficiently.

(**a**)

(**b**)

(**c**)
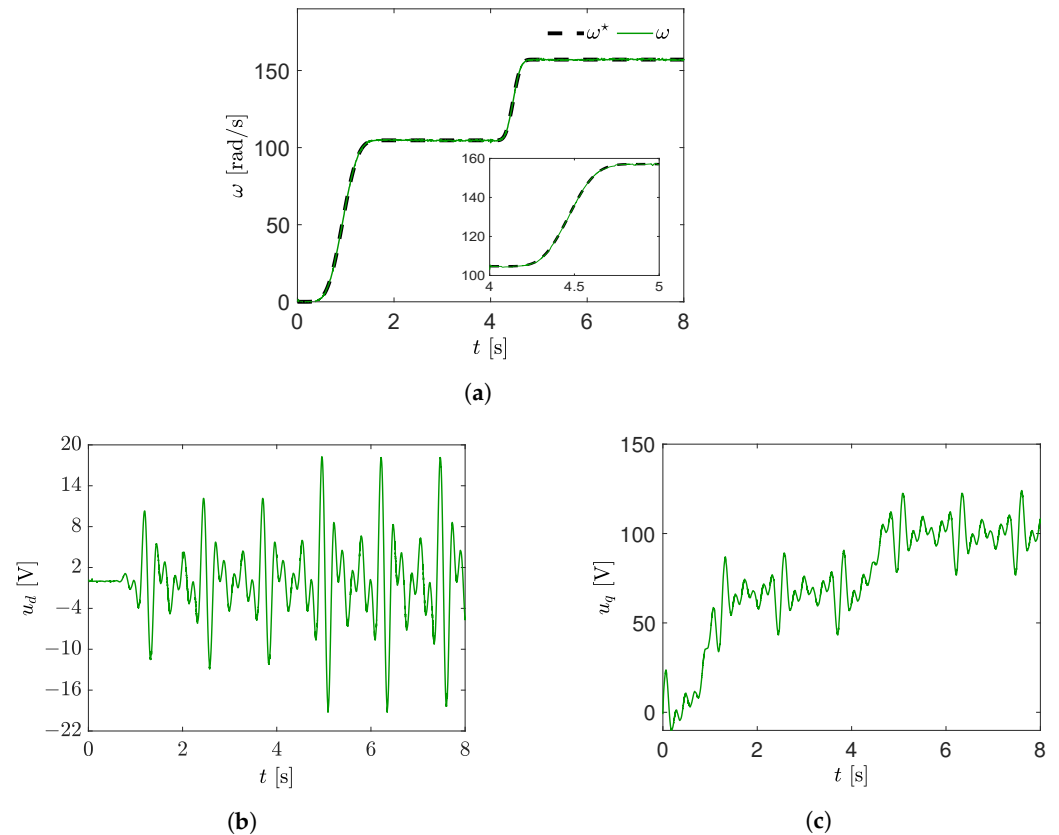
Figure 10. Motor synchronous control parameter output using the general approximation (7). (**a**) Speed response with chattering phenomenon reduction, first trajectory planned, and synchronous motor speed response. (**b**) Voltage generated in direct axis, (**c**) voltage generated in quadrature axis.

The adjustment of ϵ ensures that the resulting function closely approximates the sign function while maintaining a smooth transition around zero, effectively alleviating the adverse impact of chattering in the control system. Subsequently, the version from (8) is employed as Figure 11 shows; this function presents a better behavior, practically eliminating these undesired oscillations, as can also be seen in the control voltages in Figure 11b,c. For these cases, $\epsilon = 900$ for approximations described by the rest of Equations (9)–(13).

By evaluating approximation hyperbolic tangent, it can be observed that ϵ should be increased since the phenomenon is still present in the system's response, as displayed in Figure 12. Control voltages are in the same situation in Figure 12b,c.
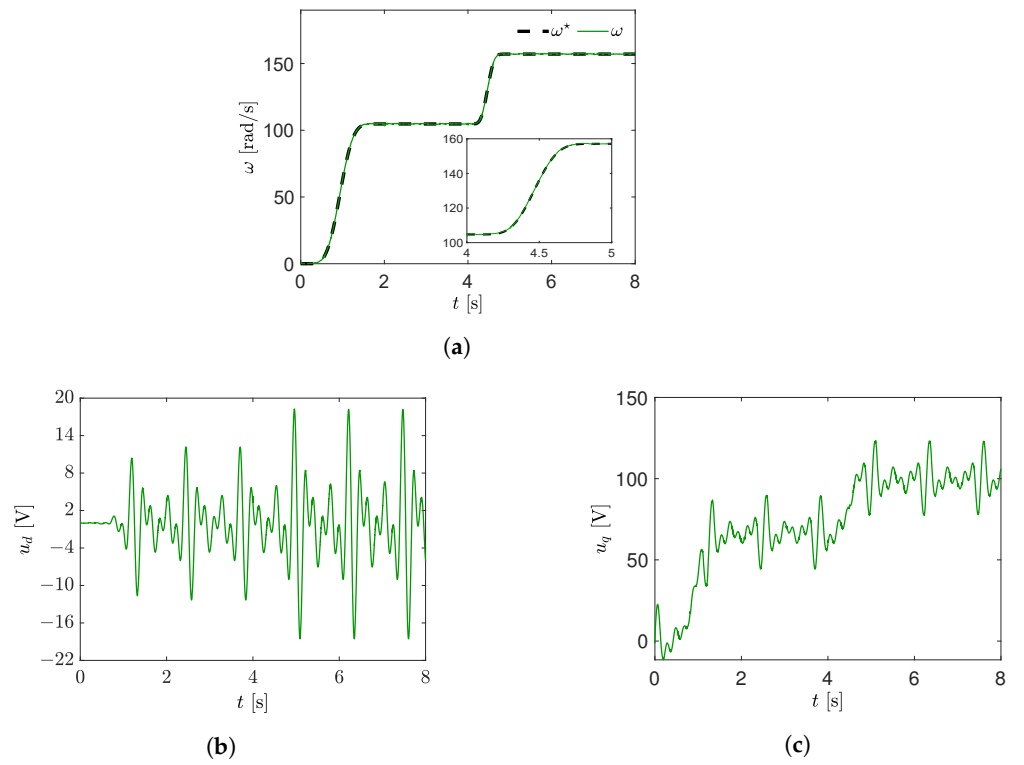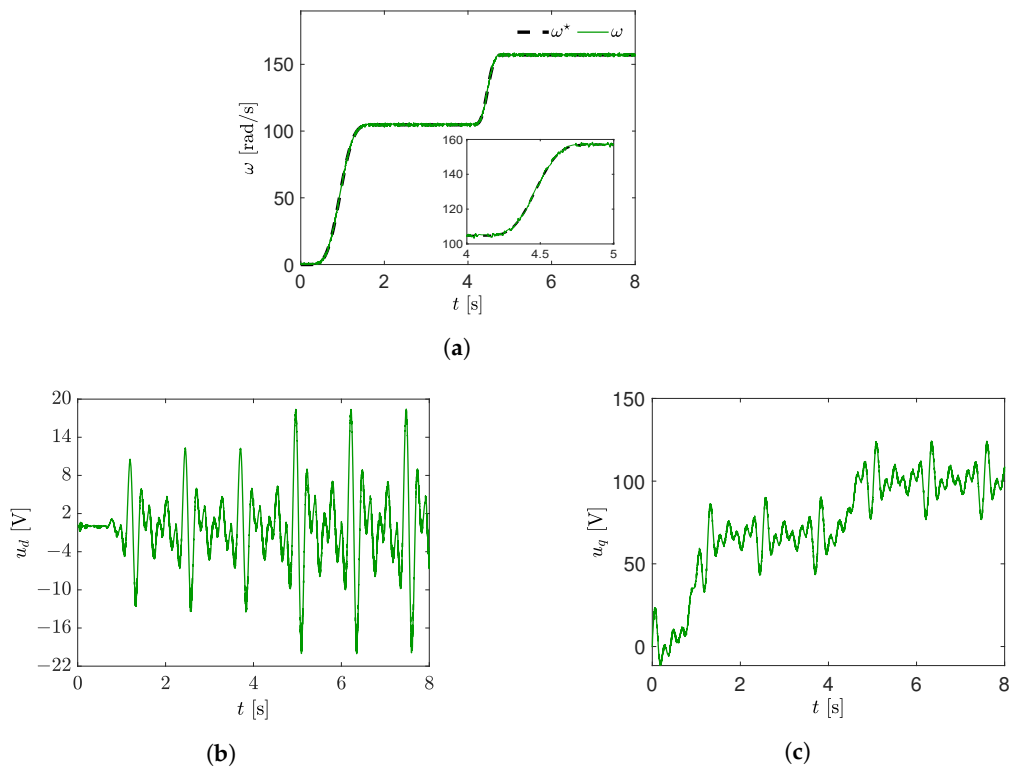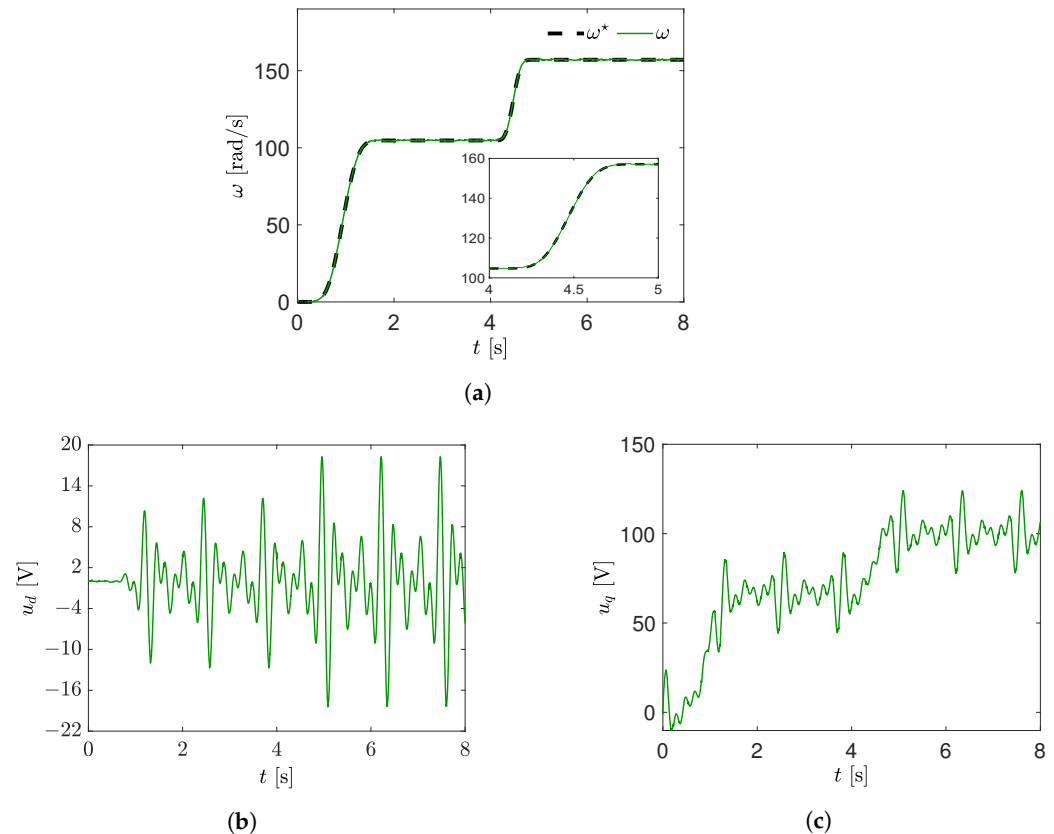
(a)

(b)

(c)

Figure 11. Motor synchronous control parameter output using the general approximation from (8). (**a**) Speed response with chattering phenomenon reduction, first trajectory planned, and synchronous motor speed response. (**b**) Voltage generated in direct axis, (**c**) Voltage generated in quadrature axis.

(a)

(b)

(c)

Figure 12. Motor synchronous control parameter output using hyperbolic tangent function from (9). (**a**) Speed response with chattering phenomenon reduction, first trajectory planned, and synchronous motor speed response. (**b**) Voltage generated in direct axis, (**c**) voltage generated in quadrature axis.

The approximation arc tangent and the general approximation (10) are implemented, revealing a favorable behavior in the system's response. The speed response, showcased in Figure 13a, distinctly demonstrates good behavior. This desirable property extends to the control signals depicted in Figure 13b,c, displaying minimal chattering in both u_d and u_q voltages. Despite minimal oscillations observed in the final approximation, this version is a solid choice for integration into the SMC.

(a)

(b)

(c)

Figure 13. Motor synchronous control parameter output using arc tangent approximation from (10). (**a**) Speed response with minimum chattering phenomenon, first trajectory planned, and synchronous motor speed response. (**b**) Voltage generated in direct axis, (**c**) voltage generated in quadrature axis.

The general approximation (12) is a variation from (11), [14]. Taking the same ϵ value for both functions demonstrates that the general approximation (12) shows a better behavior versus the previous version, visible when responses in Figures 14 and 15 are compared, and chattering is notably reduced.

Although the saturation function (13) is widely reported to address this issue in the sliding mode control, the previous options can also be considered according to the system's needs. For the ϵ value used in the first study case, the saturation function is the one that best suppresses the chattering, as depicted in Figure 16, due to the slope.
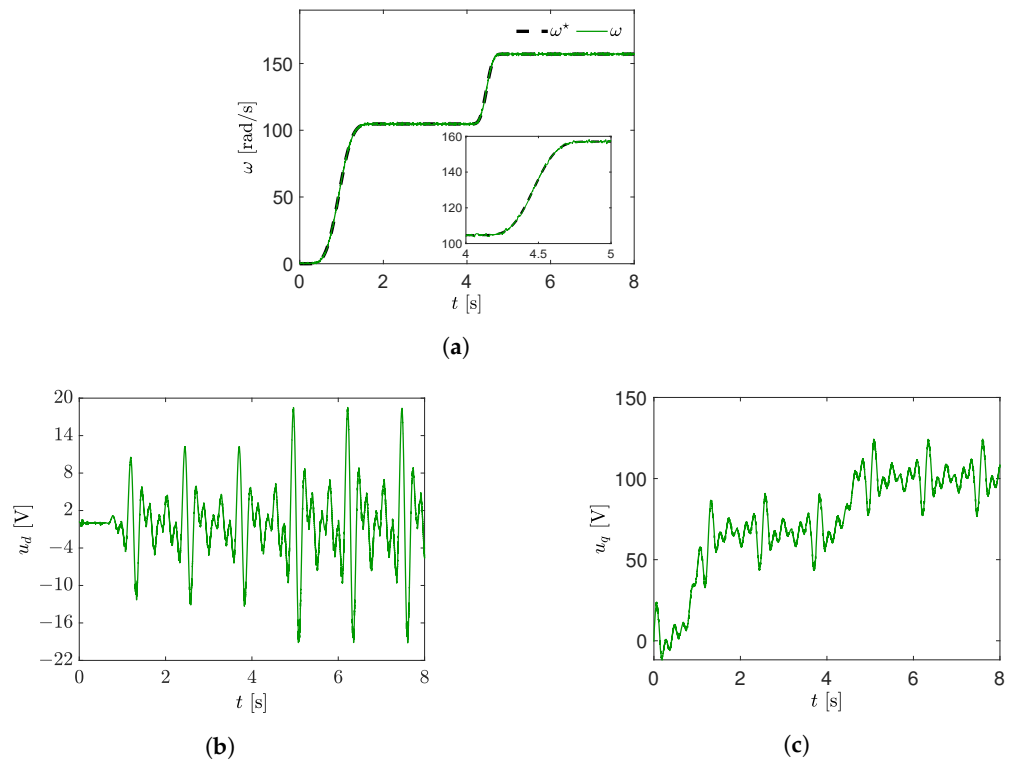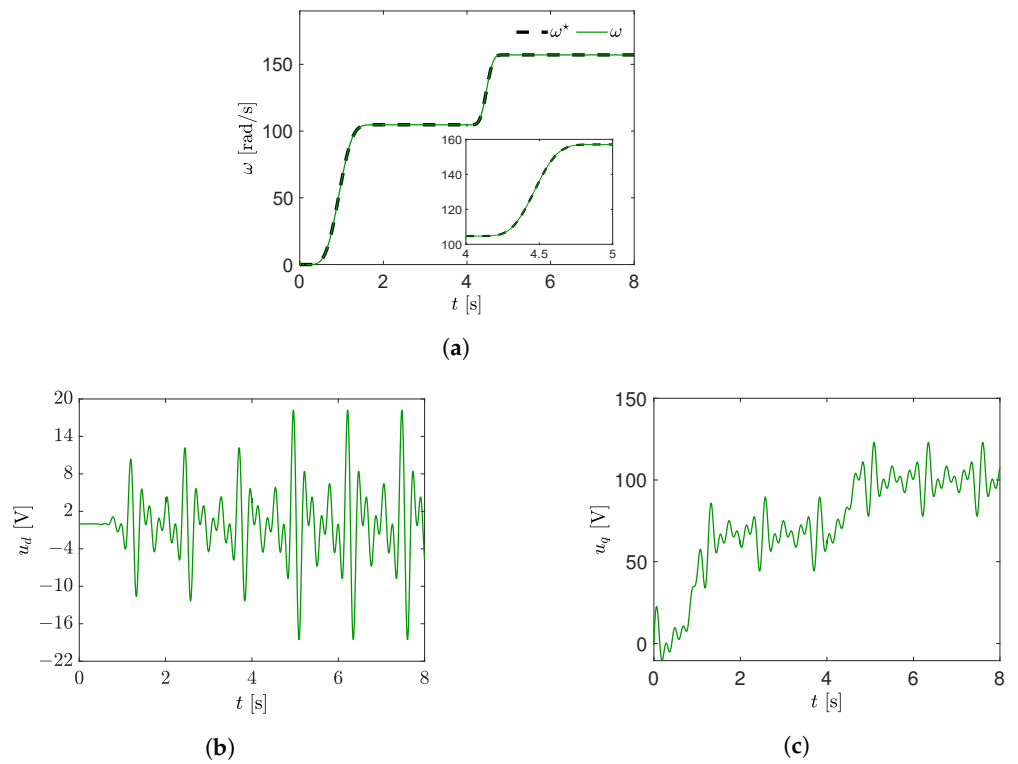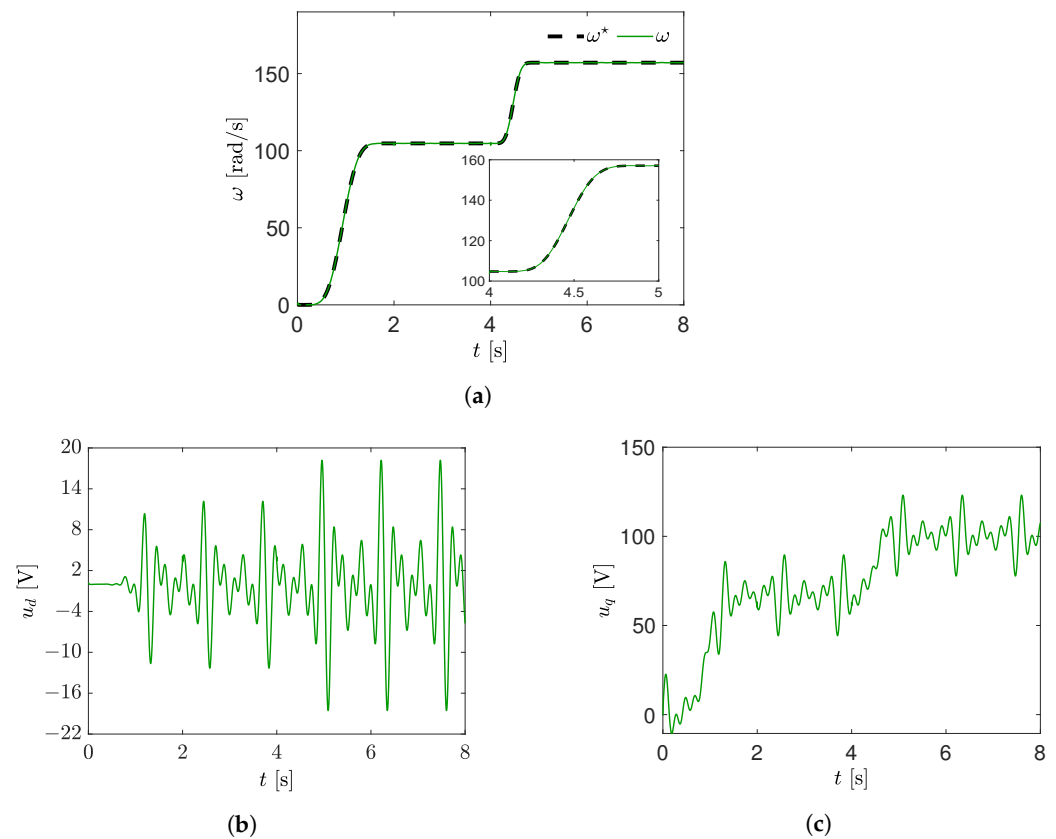
(**a**)

(**b**)

(**c**)

Figure 14. Motor synchronous control parameter output using the general approximation from (11). (**a**) Speed response with chattering phenomenon, first trajectory planned, and synchronous motor speed response. (**b**) Voltage generated in direct axis, (**c**) voltage generated in quadrature axis.

(**a**)

(**b**)

(**c**)

Figure 15. Motor synchronous control parameter output using the general approximation from Equation (12). (**a**) Speed response with chattering phenomenon, first trajectory planned, and synchronous motor speed response. (**b**) Voltage generated in direct axis, (**c**) voltage generated in quadrature axis.

Figure 16. Motor synchronous control parameter output using The saturation function from (13). (**a**) Speed response with chattering phenomenon reduction, first trajectory planned, and synchronous motor speed response. (**b**) Voltage generated in direct axis, (**c**) voltage generated in quadrature axis.

4.3. Control Speed Evaluation for the Second Speed Trajectory

A second study case was conducted with a new proposed load torque speed trajectory, shown in Figure 17, described by Equation (34) and a new speed trajectory shown in Figure 18 described again by Equation (32), with parameters shown in Table 3.

$$\tau_L = \sum_{i=1}^{4} A_i \sin(\omega_i t) \tag{34}$$

Table 3. Paramete values of the second proposed load torque as an oscillation addition.

Parameter	Value
Amplitude	(Nm)
A_1	1
A_2	1.5
A_3	3
A_4	1
Frequency	(rad/s)
ω_1	5
ω_2	15
ω_3	25
ω_4	5

With speed references $\overline{\omega}_1 = 0$ rad/s, $\overline{\omega}_2 = 209.44$ rad/s (2000 rpm), $\overline{\omega}_3 = 104.719$ rad/s (1000 rpm), $t_1 = 0$ s, $t_2 = 2$ s, $t_3 = 4$ s, $t_4 = 5$ s. Firstly, $sign_1(\sigma)$ is evaluated in the control scheme shown in Figure 19; for this new trajectory, the control performs optimally by tracking the speed trajectory, and once again, control signals in Figure 19b,c show chattering due to the standard sign function.
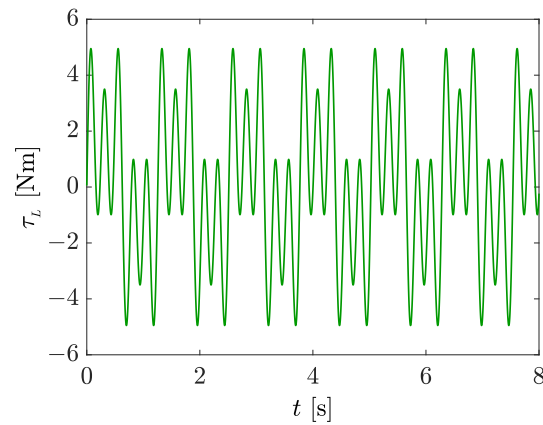
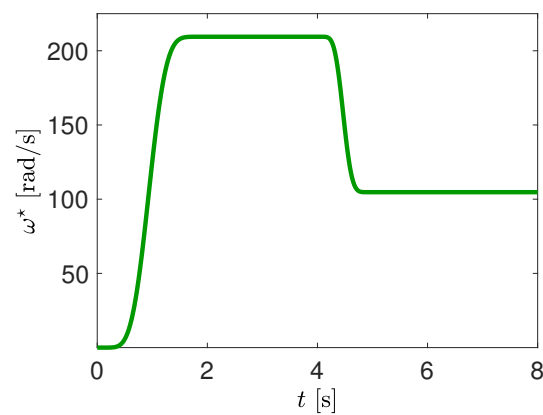**Figure 17.** Load torque proposed for the second study case.

Figure 18. Speed reference trajectory for the second study case.

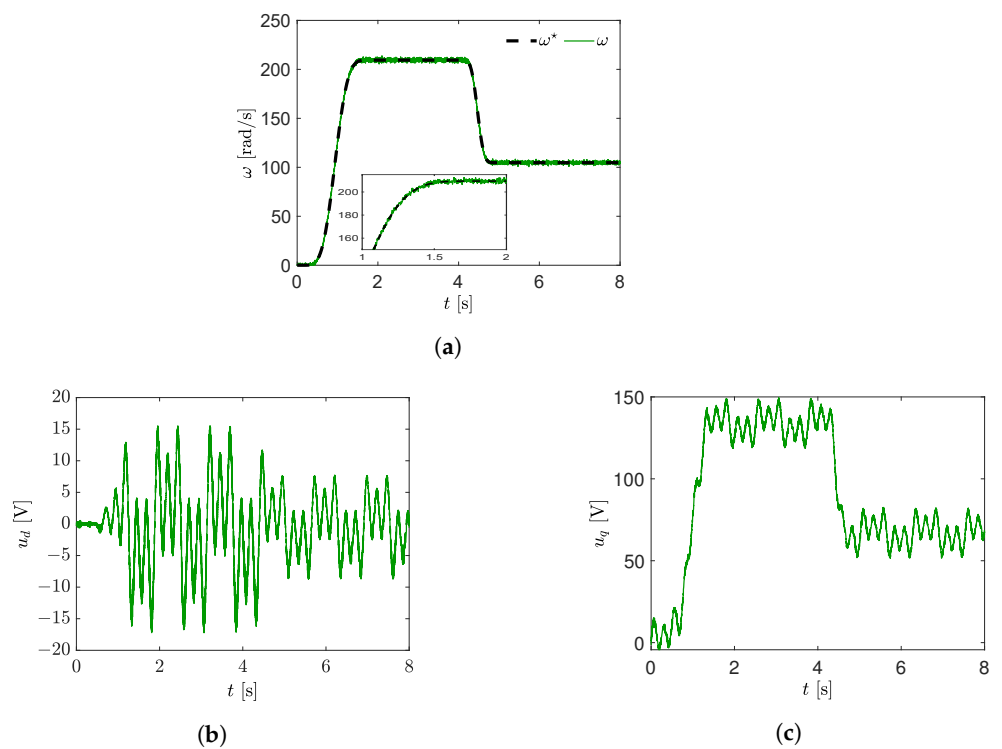(**a**)

(**b**)

(**c**)

Figure 19. Motor synchronous control parameter output using standard sign function from (1). (**a**) Speed response with chattering phenomenon, second trajectory planned, and synchronous motor speed response. (**b**) Voltage generated in direct axis, (**c**) voltage generated in quadrature axis.

4.4. Sign Function Approximation Evaluation with the Second Speed Trajectory

For this case, ϵ is strategically increased to 1100 to obtain a smoother slope in each approximation; notice that this is the only parameter that should be modified, and the control law should be kept the same. As in the previous case, the control scheme keeps its robustness and efficiency, and it is displayed in Figures 20–24, where approximation from Equation (7) is employed. Notice that in this specific case, chattering is practically suppressed. In contrast with the previous approximations (7), (10), (12) and (13) show the best performance in almost suppressing this phenomenon.

The approximation from Equation (12) shows a better response in suppressing this phenomenon in contrast with Equation (11), noticeable when Figures 24 and 25 are compared. The saturation function from Equation (13) is effective since the slope is a little more pronounced than others. However, if the epsilon value is inappropriate, the slope is minimal, and its values are almost the same as the standard sign function. As Figure 26 demonstrates, the ϵ value used, in this case, suppresses chattering almost totally.
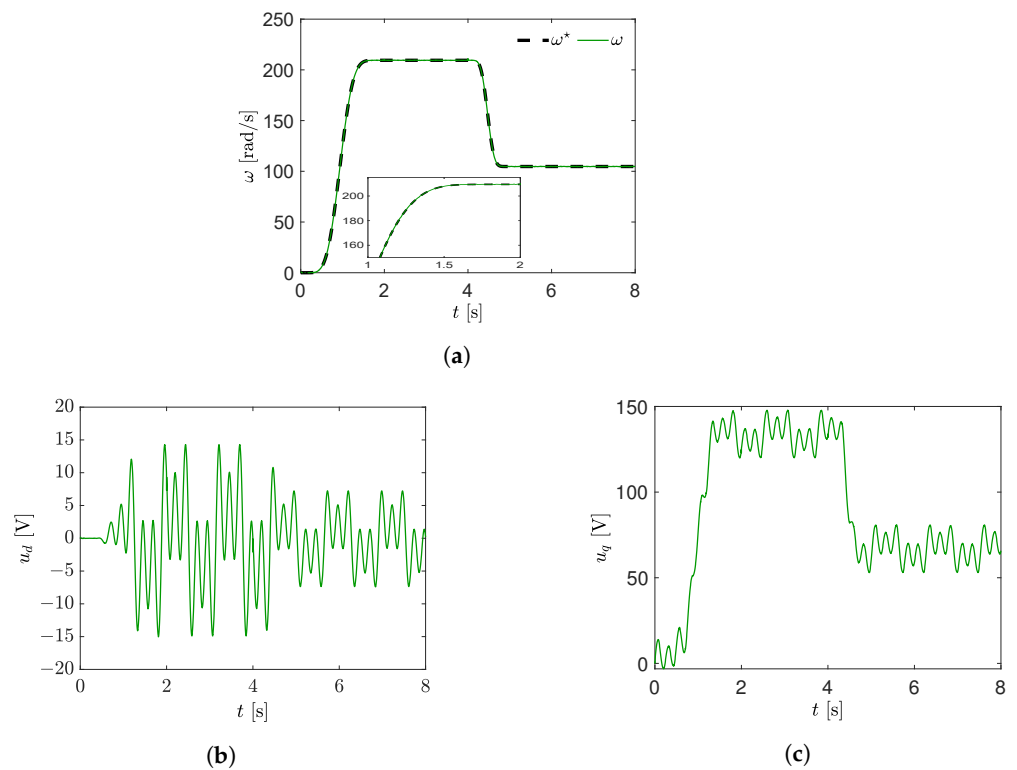

(a)

(b)

(c)

Figure 20. Motor synchronous control parameter output using approximation from Equation (7). (**a**) Speed response with chattering phenomenon suppressed, second trajectory planned, and synchronous motor speed response. (**b**) Voltage generated in direct axis, (**c**) voltage generated in quadrature axis.
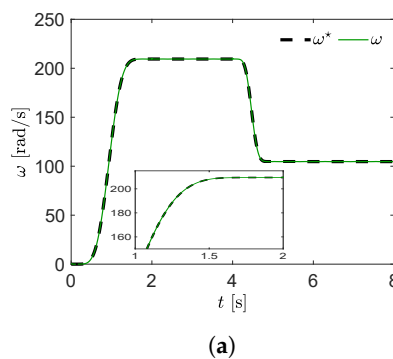

(a)

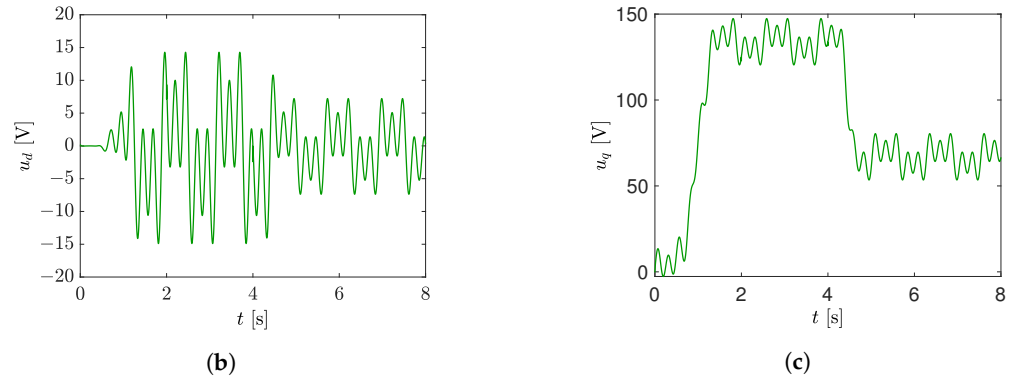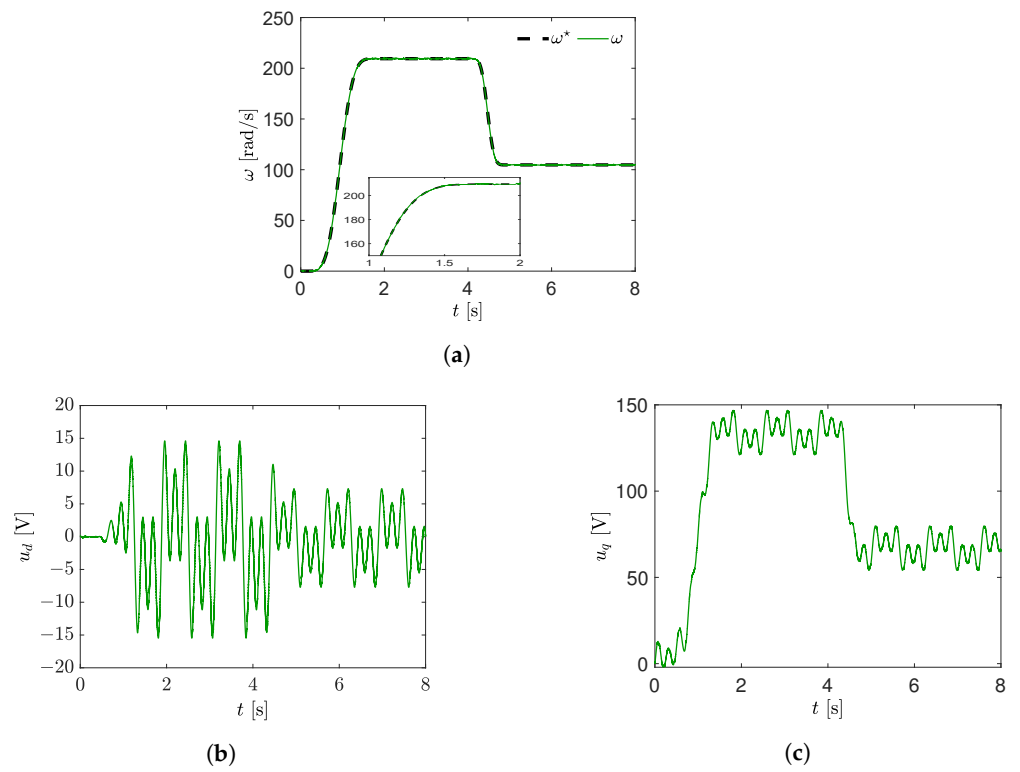**Figure 21.** *Cont.*

(**b**)

(**c**)

Figure 21. Motor synchronous control parameter output using approximation from (8). (**a**) Speed response with chattering phenomenon suppressed, second trajectory planned, and synchronous motor speed response. (**b**) Voltage generated in direct axis, (**c**) voltage generated in quadrature axis.
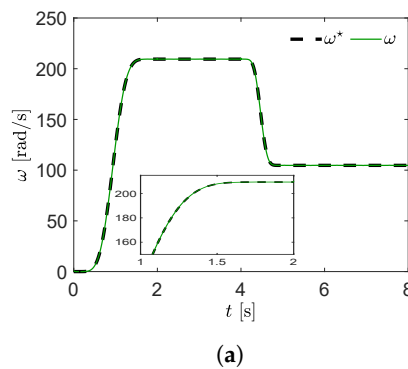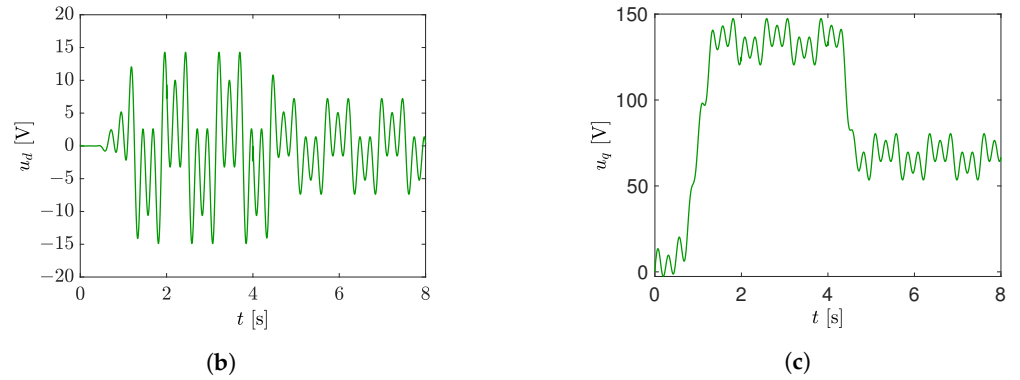

(**a**)

(**b**)

(**c**)

Figure 22. Motor synchronous control parameter output using approximation from (9). (**a**) Speed response with chattering phenomenon reduction, second trajectory planned, and synchronous motor speed response. (**b**) Voltage generated in direct axis, (**c**) voltage generated in quadrature axis.

(**a**)

Figure 23. *Cont.*

(**b**)

(**c**)

Figure 23. Motor synchronous control parameter output using approximation from (10). (**a**) Speed response with chattering phenomenon suppressed, second trajectory planned, and synchronous motor speed response. (**b**) Voltage generated in direct axis, (**c**) voltage generated in quadrature axis.
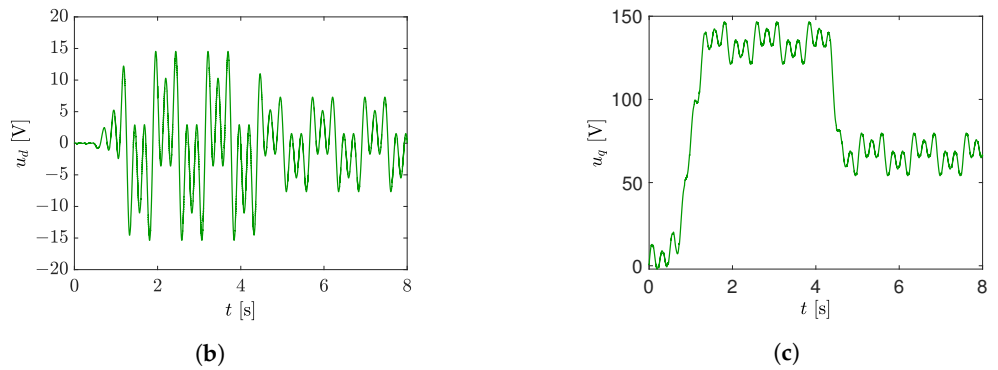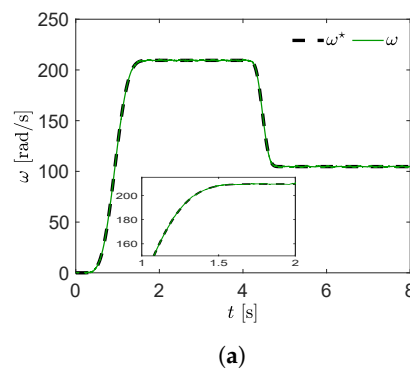

(**a**)

(**b**)

(**c**)

Figure 24. Motor synchronous control parameter output using approximation from (11). (**a**) Speed response with chattering phenomenon, second trajectory planned, and synchronous motor speed response. (**b**) Voltage generated in direct axis, (**c**) voltage generated in quadrature axis.

(**a**)

Figure 25. *Cont*.

(b)

(c)

Figure 25. Motor synchronous control parameter output using approximation from (12). (**a**) Speed response with chattering phenomenon suppressed, second trajectory planned, and synchronous motor speed response. (**b**) Voltage generated in direct axis, (**c**) voltage generated in quadrature axis.
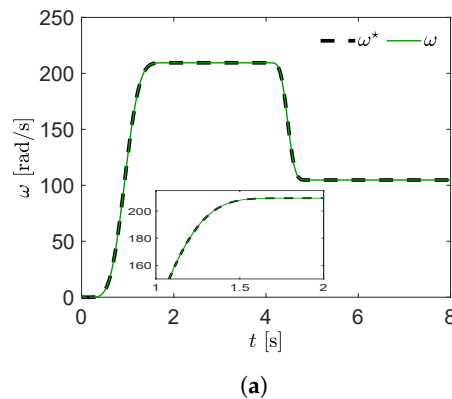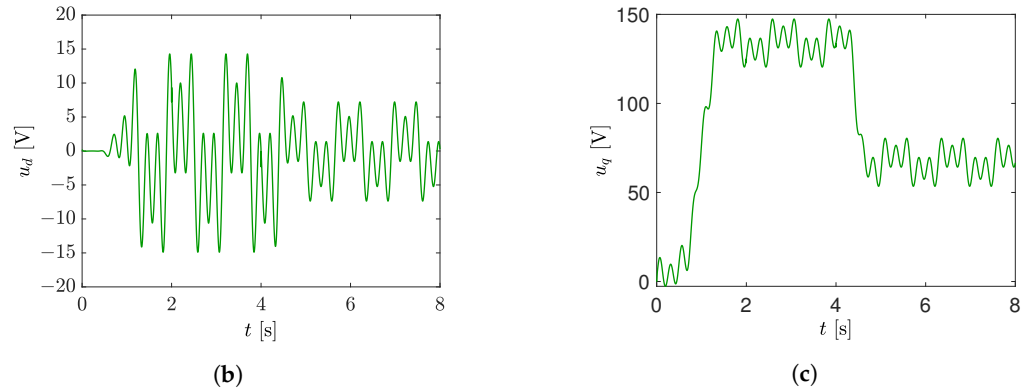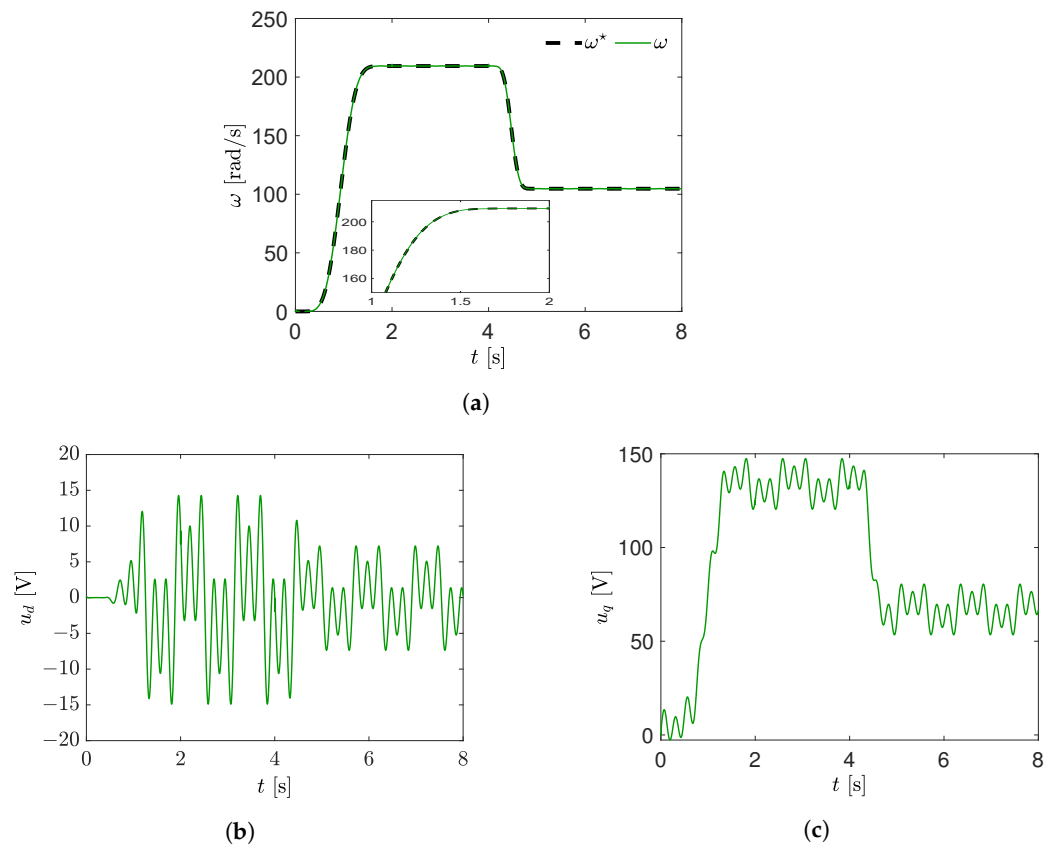

(a)

(b)

(c)

Figure 26. Motor synchronous control parameter output using saturation function (13). (**a**) Speed response with chattering phenomenon suppressed, second trajectory planned, and synchronous motor speed response. (**b**) Voltage generated in direct axis, (**c**) voltage generated in quadrature axis.

The results obtained in this study validate the proposed control scheme; the integral compensation increases the control robustness against dynamical disturbances, as observed in the generated voltages. Control gains take the values $\alpha_d = 30$, $\alpha_q = 20\omega_4$, $W_d = 80$ and $W_q = 6.5 \times 10^6$. Moreover, the system response shows an improved behavior in increment or reduction in speed trajectory transitions. This feature allows for applications where the motor must operate at different speeds. Also, various continuous sign function versions were tested in the control scheme to suppress the chattering phenomenon. It is important to notice that Equations (7)–(9), (11) and (13) show the best behavior in the control scheme, since almost a total elimination of this phenomenon is observed for the speed trajectories proposed. A bigger ϵ value results in a steeper slope for the sign

function approximation. This approach keeps the control law easy to implement where approximations have to be programmed. The adaptive super-twisting reaching law can effectively suppress chattering [3]. However, the computational cost increases and is complex to implement. In this way, the use of sign function approximations allows for keeping the control law and selecting diverse sliding surfaces. In addition, the approach proposed in [6] involves two control law superpositions to address this phenomenon. The presence of uncertain disturbances must be considered within the control design where different approaches are limited.

5. Conclusions

This study introduced an innovative chattering suppression approach for a sliding mode control scheme for tracking speed trajectories for a PMSM. The technique has improved by adding integral compensation, showed a good response against variable torque loads and speed reference changes incorporated with Bezier curves. The suppression of the chattering phenomenon was achieved using sign function approximations, and the importance of mitigating this issue relies on the best system performance. The results revealed a notable reduction; in some instances, this phenomenon was eliminated. Through several evaluations, each approximation was employed for the proposed references. Manipulating the ϵ parameter in sign function approximations allows for adjusting the function slope, resulting in a reduced chattering in control response. The versatility of this methodology extends its applicability to diverse sliding mode control designs, making it a valuable tool for a wide array of applications, including agriculture systems. For future work, the experimental implementation of this controller will be conducted in applications such as agriculture machinery with a new approximation to eliminate the chattering phenomenon. Moreover, the importance of tuning a specific ϵ parameter for the approximations will be addressed with neural networks to improve the control strategy, as was proposed in [21].

Author Contributions: Conceptualization, D.M.-A., F.B.-C., I.R.-C., H.Y.-B., A.F.-C. and J.C.R.-C.; methodology, D.M.-A., F.B.-C. and A.F.-C.; software, D.M.-A., F.B.-C., I.R.-C. and H.Y.-B.; validation, D.M.-A., F.B.-C., I.R.-C., A.F.-C.; formal analysis, F.B.-C., I.R.-C., H.Y.-B., A.F.-C. and J.C.R.-C.; investigation, D.M.-A., F.B.-C., I.R.-C. and A.F.-C.; resources, F.B.-C., A.F.-C., I.R.-C. and J.C.R.-C.; data curation, D.M.-A., F.B.-C. and H.Y.-B.; writing—original draft preparation, D.M.-A., F.B.-C., I.R.-C., H.Y.-B., A.F.-C. and J.C.R.-C.; writing—review and editing, D.M.-A., F.B.-C., I.R.-C. and H.Y.-B.; visualization, D.M.-A., F.B.-C. and I.R.-C.; supervision, F.B.-C. and I.R.-C.; project administration, F.B.-C.; funding acquisition, F.B.-C. and I.R.-C. All authors have read and agreed to the published version of the manuscript.

Conflicts of Interest: The authors declare no conflicts of interest.

References

1. Zhang, D.; Zhang, H.; Li, X.; Zhao, H.; Zhang, Y.; Wang, S.; Ahmad, T.; Liu, T.; Shuang, F.; Wu, T. A PMSM control system for electric vehicle using improved exponential reaching law and proportional resonance theory. *IEEE Trans. Veh. Technol.* **2023**, *72*, 8566–8578. [CrossRef]
2. Akhil, R.S.; Mini, V.P.; Mayadevi, N.; Harikumar, R. Modified flux-weakening control for electric vehicle with PMSM drive. *IFAC-PapersOnLine* **2020**, *53*, 325–331. [CrossRef]
3. Gao, P.; Zhang, G.; Ouyang, H.; Mei, L. An adaptive super twisting nonlinear fractional order PID sliding mode control of permanent magnet synchronous motor speed regulation system based on extended state observer. *IEEE Access* **2020**, *8*, 53498–53510. [CrossRef]

4. Zellouma, D.; Benbouhenni, H.; Bekakra, Y. Backstepping control based on a third-order sliding mode controller to regulate the torque and flux of asynchronous motor drive. *Period. Polytech. Electr. Eng. Comput. Sci.* **2023**, *67*, 10–20. [CrossRef]

5. Levant, A. Chattering analysis. *IEEE Trans. Autom. Control* **2010**, *55*, 1380–1389. [CrossRef]

6. Feng, Y.; Han, F.; Yu, X. Chattering free full-order sliding-mode control. *Automatica* **2014**, *50*, 1310–1314. [CrossRef]

7. Vinh, V.Q.; Ha, V.T. Improved Torque Ripple of Switched Reluctance Motors using Sliding Mode Control for Electric Vehicles. *Eng. Technol. Appl. Sci. Res.* **2023**, *13*, 10140–10144. [CrossRef]

8. Chavez-Conde, E.; Beltrán-Carbajal, F.; Blanco-Ortega, A.; Mendez-Azua, H. Sliding mode and Generalized PI control of vehicle active suspensions. In Proceedings of the 2009 IEEE Control Applications, (CCA) & Intelligent Control, (ISIC), St. Petersburg, Russia, 8–10 July 2009; pp. 1726–1731. [CrossRef]

9. Yuan, L.; Jiang, Y.; Xiong, L.; Wang, P. Sliding Mode Control Approach with Integrated Disturbance Observer for PMSM Speed System. *CES Trans. Electr. Mach. Syst.* **2023**, *7*, 118–127. [CrossRef]

10. Sehab, R.; Akrad, A.; Saadi, Y. Super-Twisting Sliding Mode Control to Improve Performances and Robustness of a Switched Reluctance Machine for an Electric Vehicle Drivetrain Application. *Energies* **2023**, *16*, 3212. [CrossRef]

11. Tarchala, G.; Orlawska-Kowalska, T. Sliding mode speed observer for the induction motor drive with different sign function approximation forms and gain adaptation. *Organ Stowarzyszenia Elektr. Pol.* **2013**, *1*, 13. Available online: http://pe.org.pl/articles/2013/1a/1.pdf (accessed on 10 April 2024).

12. Sadeghi, M.; Ghayem, F.; Babaie-Zadeh, M.; Chatterjee, S.; Skoglund, M.; Jutten, C. LOSoft: l0 Minimization via Soft Thresholding. In Proceedings of the 2019 27th European Signal Processing Conference (EUSIPCO), A Coruna, Spain, 2–6 September 2019; pp. 1–5. [CrossRef]

13. Kyurkchiev, V.; Kyurkchiev, N. A family of recurrence generated functions based on the half-hyperbolic tangent activation function. *Biomed. Stat. Inform.* **2017**, *2*, 87–94. [CrossRef]

14. Shokouhi, F.; Davaie Markazi, A.H. A new continuous approximation of sign function for sliding mode control. In Proceedings of the International Conference on Robotics and Mechatronics (ICRoM 2018), Tehran, Iran, 23–25 October 2018. Available online: https://www.researchgate.net/profile/Farbood-Shokouhi/publication/328130695_A_new_continuous_approximation_of_sign_function_for_sliding_mode_control/links/5bb9ccf0a6fdcc9552d5667b/A-new-continuous-approximation-of-sign-function-for-sliding-mode-control.pdf (accessed on 10 April 2024).

15. Nise, N.S. *Control Systems Engineering*, 7th ed.; John Wiley & Sons: Pomona, CA, USA, 2015.

16. Utkin, V.; Guldner, J.; Shi, J. *Sliding Mode Control in Electro-Mechanical Systems*, 2nd ed.; CRC Press: Boca Raton, FL, USA, 2009.

17. Edwards, C.; Spurgeon, S. *Sliding Mode Control: Theory and Applications*, 1st ed.; CRC Press: Boca Raton, FL, USA, 1998.

18. Prakosa, J.A.; Purwowibowo, P.; Kurniawan, E.; Wijonarko, S.; Maftukhah, T.; Rustandi, D.; Pratiwi, E.B.; Rahmanto, R. Experimental Design of Fast Terminal Sliding Mode Control for Valve Regulation under Water Load Uncertainty for Precision Irrigation. *Actuators* **2023**, *12*, 155. [CrossRef]

19. Beltran-Carbajal, F.; Tapia-Olvera, R.; Lopez-Garcia, I.; Valderrabano-Gonzalez, A.; Rosas-Caro, J.C.; Hernandez-Avila, J.L. Extended PI feedback tracking control for synchronous motors. *Int. J. Control Autom. Syst.* **2019**, *17*, 1346–1358. . [CrossRef]

20. Beltran-Carbajal, F.; Favela-Contreras, A.; Hernandez-Avila, J.L.; Olvera-Tapia, O.; Sotelo, D.; Sotelo, C. Dynamic output feedback control for desired motion tracking on synchronous motors. *Int. Trans. Electr. Energy Syst.* **2020**, *30*, e12260. . [CrossRef]

21. Beltran-Carbajal, F.; Yañez-Badillo, H.; Tapia-Olvera, R.; Rosas-Caro, J.C.; Sotelo, C.; Sotelo, D. Neural Network Trajectory Tracking Control on Electromagnetic Suspension Systems. *Mathematics* **2023**, *11*, 2272. [CrossRef]

22. Cheng, S.; Yu, J.; Zhao, L.; Ma, Y. Adaptive fuzzy control for permanent magnet synchronous motors considering input saturation in electric vehicle stochastic drive systems. *J. Frankl. Inst.* **2020**, *357*, 8473–8490. [CrossRef]

23. An Y.; Wang, L.; Deng, X.; Chen, H.; Lu, Z.; Wang, T. Research on Differential Steering Dynamics Control of Four-Wheel Independent Drive Electric Tractor. *Agriculture* **2023**, *13*, 1758. [CrossRef]

24. Lu, E.; Xue, J.; Chen, T.; Jiang, S. Robust Trajectory Tracking Control of an Autonomous Tractor-Trailer Considering Model Parameter Uncertainties and Disturbances. *Agriculture* **2023**, *13*, 869. [CrossRef]

25. Sun, C.; Sun, P.; Zhou, J.; Mao, J. Travel reduction control of distributed drive electric agricultural vehicles based on multi-information fusion. *Agriculture* **2022**, *12*, 70. [CrossRef]

26. Wang, H.; Zhao, J.; Zhang, L.; Yu, S. Application of Disturbance Observer-Based Fast Terminal Sliding Mode Control for Asynchronous Motors in Remote Electrical Conductivity Control of Fertigation Systems. *Agriculture* **2024**, *14*, 168. . [CrossRef]

27. Xiong, H.; Zhang, M.; Zhang, R.; Zhu, X.; Yang, L.; Guo, X.; Cai, B. A new synchronous control method for dual motor electric vehicle based on cognitive-inspired and intelligent interaction. *Future Gener. Comput. Syst.* **2019**, *94*, 536–548. . [CrossRef]

28. Sain, C.; Banerjee, A.; Biswas, P.K. Modelling and comparative dynamic analysis due to demagnetization of a torque controlled permanent magnet synchronous motor drive for energy-efficient electric vehicle. *ISA Trans.* **2020**, *97*, 384–400. [CrossRef] [PubMed]

29. Ullah, K.; Guzinski, J.; Mirza, A.F. Critical review on robust speed control techniques for permanent magnet synchronous motor (PMSM) speed regulation. *Energies* **2022**, *15*, 1235. [CrossRef]

30. Xia, X.; Zhang, B.; Li, X. High precision low-speed control for permanent magnet synchronous motor. *Sensors* **2020**, *20*, 1526. [CrossRef] [PubMed]

31. Wang, Z.; Yao, B.; Guo, L.; Jin, X.; Li, X.; Wang, H. Initial rotor position detection for permanent magnet synchronous motor based on high-frequency voltage injection without filter. *World Electr. Veh. J.* **2020**, *11*, 71. [CrossRef]

32. Beltran-Carbajal, F.; Favela-Contreras, A.; Lopez-Garcia, I.; Valderrabano-Gonzalez, A.; Rosas-Caro, J.C.; Sanchez-Huerta, V.M. Output feedback dynamic tracking excitation control of synchronous generators. *IET Gener. Transm. Distrib.* **2016**, *10*, 3041–3049. [CrossRef]

33. Huang, A.; Chen, Z.; Wang, J. Research on the dq-Axis Current Reaction Time of an Interior Permanent Magnet Synchronous Motor for Electric Vehicle. *World Electr. Veh. J.* **2023**, *14*, 196. [CrossRef]

34. Suman, K.; Mathew, A.T. Speed control of permanent magnet synchronous motor drive system using PI, PID, SMC and SMC plus PID controller. In Proceedings of the 2018 International Conference on Advances in Computing, Communications and Informatics (ICACCI), Bangalore, India, 19–22 September 2018; pp. 543–549. [CrossRef]

35. Andrade, D.M.; Carbajal, F.B.; Cruz, J.E.E.; Cambero, I.D.J.R.; Pérez, A.C. Control de velocidad basado en modos deslizantes con aproximaciones de la función signo para un motor síncrono (speed control based on sliding modes with sign function approximations for a synchronous motor). *Pist. Educ.* **2023**, *45*, 626–642. Available online: https://pistaseducativas.celaya.tecnm. mx/index.php/pistas/article/view/3397/2472 (accessed on 10 April 2024).

36. Chen, Z.; Dai, X.; Faizan, M. Speed Stability and Anti-Disturbance Performance Improvement of an Interior Permanent Magnet Synchronous Motor for Electric Vehicles. *World Electr. Veh. J.* **2023**, *14*, 311. [CrossRef]

37. Gao, W.; Zhang, G.; Hang, M.; Cheng, S.; Li, P. Sensorless Control Strategy of a Permanent Magnet Synchronous Motor Based on an Improved Sliding Mode Observer. *World Electr. Veh. J.* **2021**, *12*, 74. [CrossRef]

38. Lu, E.; Li, W.; Wang, S.; Zhang, W.; Luo, C. Disturbance rejection control for PMSM using integral sliding mode based composite nonlinear feedback control with load observer. *ISA Trans.* **2021**, *116*, 203–217. [CrossRef] [PubMed]